



## Optimization of methylene blue and povidone-iodine adsorption conditions on activated biochar from sunflower husk pyrolysis

Beata Jabłońska<sup>a,\*</sup>, Maciej Gliniak<sup>b</sup>

<sup>a</sup>Faculty of Infrastructure and Environment, Institute of Environmental Engineering, Czestochowa University of Technology, Brzeźnicka St. 60a, 42-200 Czestochowa, Poland, email: beata.jablonska@pcz.pl

<sup>b</sup>Faculty of Production and Power Engineering, University of Agriculture in Krakow, Mickiewicza Av. 21, 31-120 Kraków, Poland, email: maciej.gliniak@ur.krakow.pl

Received 31 December 2022; Accepted 5 April 2023

### ABSTRACT

Commercial activated carbons are mainly used in the adsorption process to remove pollutants from water and wastewater, however, due to their high costs, substitutes are currently being sought. Carbon materials obtained from activated biomass often show a high specific surface area (similar to that for activated carbons) due to a well-developed pore structure. In this study, activated biochar obtained from sunflower husks was tested for the adsorption of povidone-iodine (PVP-I) and methylene blue (MB). The biochar was prepared in the pyrolysis process (500°C) and chemically activated with  $K_2CO_3$  at a temperature of 800°C. The activation affected greatly the structural properties of the biochar – the specific surface area increased from 32.5 to 740.5  $m^2/g$ , and the micropore and mesopore volume increased over 20 and 15 times, respectively. Also the iodine value changed from 89 to 495  $mg/g$ . The physicochemical and granulometric properties as well as pH value of point of zero charge of the adsorbent surface were determined. The central composite design method was used to determine the optimal adsorption conditions (solution pH and adsorbent mass) in the initial concentration range 10–60  $mg/dm^3$  for PVP-I and 30–250  $mg/dm^3$  for MB. The maximum sorption capacity reaches 120  $mg/g$  for MB and 5.6  $mg/g$  for PVP-I. Sorption kinetics was investigated with use of several models. The times of half-saturation for these adsorbates are around 1 and 15 min, respectively. The detected Gibbs free energy change indicates the adsorption is spontaneous and thermodynamically favored. The adsorptive properties of the biochar obtained from waste sunflower husk are especially good for MB adsorption and acceptable with respect to PVP-I adsorption.

*Keywords:* Adsorption; Sunflower husk; Pyrolysis; Chemical activation; Povidone-iodine; Methylene blue

### 1. Introduction

In the last decade, thanks to significantly tightened regulations on pollutants from industry and agriculture, and new significantly improved technologies for water and wastewater treatment, Europe has taken a big step towards reducing emissions into the environment. Nevertheless, water pollution is still a serious problem, and its excessive exploitation, industrialization and climate change still affect its quality and availability [1]. It is estimated that more

than 2 billion people worldwide still live in countries suffering from water scarcity, and a similar number of people rely on contaminated drinking water sources. This situation is also projected to worsen over the years due to further climate change and population growth [2]. Substances that get into surface and underground waters as a result of industrialization, as well as contact of waters with various wastes abandoned to the environment, are toxic and harmful to the environment. They cause many serious diseases in humans and animals. In recent years, drastic effects caused

\* Corresponding author.

by surface water contamination have been observed especially in children [3]. Water sources can be contaminated with substances such as dyes, heavy metals, pharmaceuticals and more and more new substances undetectable so far. Research by the European Environment Agency (EEA) shows that the amount of personal protection products and pharmaceuticals released into the environment each year is approximately equal to the annual use of pesticides [4].

Analyses of surface waters in Poland also confirm the constantly growing presence of dyes, pharmaceuticals and personal care products (PPCPs) in waters [5–7]. Products such as soaps, detergents, disinfectants and cosmetics are active sources of PPCPs. They are now more and more often detected in sewage treatment plants [8], surface and groundwater [9] and even in drinking water [10]. Due to the complex chemical structure, these compounds are not fully removed in the wastewater treatment process, and in the unchanged form or as intermediate metabolites, they may affect the pollution of surface and deep waters [6,11].

In recent years, due to the COVID-19 epidemic, the use of cosmetic skin disinfectants by the population has increased in particular. One such agent is the polyvinylpyrrolidone-iodine complex, commercially named as povidone-iodine (PVP-I). It is a component of cosmetic and hygienic agents, as well as pharmaceuticals. It is often added to shampoos, mousses, washing powders and other cosmetics, and during the SARS-CoV-2 epidemic it was used in hospitals as a disinfectant to prevent infections of the skin or mucous membranes [12–14]. PVP-I is an agent with a broad spectrum of antimicrobial activity, for example, against bacteria, molds and some viruses [15,16], used, for example, in the treatment of skin and mucous membranes and in washing cosmetics, for example, for hand and room decontamination [13,17]. PVP-I is classified as iodophors. It consists of iodine bound to a poly-(1-vinyl-2-pyrrolidone) carrier. It is commercially available in the form of solutions, ointments, gels and suppositories. It is characterized by high efficiency and durability. In the PVP-I solution, apart from the released free iodine, which has a disinfecting function, there is a lot of polyvinylpyrrolidone (PVP) polymer [18]. It is classified as a non-toxic polymer, but may contain unreacted residual amounts of the monomer used for polymerization, which is considered a carcinogen. In addition, synthetic polymers contained in personal care products (PCPs) and cosmetics can also be a source of environmental contamination with microplastics (MP). It has been estimated that a total of about 21.4 trillion MP particles may be released into the environment from PCPs and cosmetics annually [19]. Literature reports also cases of systemic absorption of significant amounts of PVP-I by organisms, regardless of the route of its administration, and toxic poisoning with it [20–22].

The problem of environmental pollution with dyes has also been known for a long time. Textile, chemical, paper, dyeing plants and tanneries are some of the industries that release highly colored wastewater [23]. Dyes, even in small amounts, can migrate over long distances from the source of pollution and color large volumes of water. It is estimated that about 10%–15% of the amount of dyes used in the dyeing process is discharged with sewage into the aquatic environment [24,25]. Synthetic dyes are permanent compounds, well soluble in water and poorly biodegradable

[26]. Pollution of aquatic ecosystems with dyes, even at low concentrations (below 1 mg/dm<sup>3</sup>), reduces light penetration, negatively affecting the process of photosynthesis of aquatic plants, oxygen deficiency and the life of aquatic organisms [27]. Most of the dyes are also highly poisonous and mutagenic for living organisms depending on the exposure time and concentration of the dye [28]. For example, methylene blue (MB) is a dye belonging to the group of so-called azo. It is used in the textile, paper, cosmetics, plastic dyeing and food production industries. It is believed that this dye causes allergies, can cause irritation of the digestive tract, vomiting or diarrhea [26,29,30].

The uncontrolled discharge of large amounts of PPCPs and dyes into the environment poses a major challenge to existing water and wastewater treatment technologies. There are many methods to remove PPCPs and artificial dyes from water, such as nanofiltration [31], photocatalysis [32], adsorption on activated carbons [33,34], membrane processes [35], biological treatment [36], advanced oxidation processes [37] and others. Until now, for the removal of dyes and other pollutants from water, the most used adsorbents are carbon-based materials including activated carbon [38], carbon nanotubes [39,40] and graphene [41], and natural clays [42]. In the last few years, carbon materials (biochars) produced from plant biomass have gained great importance in removing pollutants from water. Biochars are environmentally friendly and inexpensive, which is why they have become a promising adsorbent for removing pollutants from water compared to expensive activated carbons obtained from synthesized fuel precursors such as hard coal, peat or brown coal. The use of activated carbons as carbon-based adsorbents significantly increases the cost, which limits their wide application. In contrast, biochars can be produced at low cost from agricultural waste and are widely available [43]. In addition, they are made of renewable raw materials, which gives greater possibilities for the production of adsorbents. They are heterogeneous materials formed as a result of high-temperature pyrolysis of biomass, most often without access to oxygen, as well as hydrothermal carbonization, gasification or torrefaction [44]. Depending on the type of biomaterial from which they were obtained, synthesis conditions and methods of physical and chemical activation, biochars differ significantly in their physicochemical properties (e.g., specific surface area, porosity, elemental composition, etc.) [45]. The use of biochar to improve the physical properties and remediation of soil has been well documented in the literature, but not much is known about its use for drinking water treatment [46]. Currently, the use of biochar in water or wastewater treatment systems is limited. Although this material has similar properties to activated carbon, yet biochars are more heterogeneous materials obtained from different biomass. Different properties of biochars (pH, ionic strength, presence of organic matter and others) make sorption more complex [45]. The adsorption can be affected by several factors, like solution pH, adsorbent mass, adsorbate concentration, contact time, temperature and others. In the simplest approach, one-factor-at-a-time (OFAT) is considered, but more efficient approach is the response surface methodology (RSM), which detects interactions between several explanatory variables and one or more response variables. The most popular examples of RSM are factorial

designs, central composite designs (CCD) and Box–Behnken designs [47]. They differ with design of experimental points. Factorial design is simplest, but it requires many experiments, which may be impossible to carry out. In contrast, CCD offers up to 5 levels per each explanatory variable with much fewer sampling points. Moreover, the response variable can be approximated with full second-order polynomial of all explanatory variables, which allows performing optimization. Box–Behnken design is similar, but it offers three levels per explanatory variable.

Sustainable management of water resources in the world requires the provision of sufficiently clean drinking water and innovative water treatment technologies, which involves the translation of existing knowledge into economical and practical water treatment systems, including biochar technologies. Therefore, the article presents the physicochemical properties of biochar obtained as a result of pyrolysis and chemical activation of sunflower husks against sorption of methylene blue and povidone-iodine. In the next stage, optimal conditions for sorption of these compounds from water are detected. A combination of CCD and OFAT was applied: a variant of CCD was used to detect the optimal conditions with respect to solution pH, adsorbent mass and adsorbate concentration, and the impact of temperature and contact time are investigated individually.

## 2. Methodology

### 2.1. Materials

Biochar obtained from sunflower husks by pyrolysis at 450°C–550°C was used in the research, more details can be found in [48–50]. This sample was designated BC1. The obtained biochar was chemically activated using  $K_2CO_3$ . Biochar was mixed with  $K_2CO_3$  in a weight ratio of 1:3 (15 g of biochar and 45 g of  $K_2CO_3$ ) and placed in a nickel boat in a horizontal tube furnace (PRW-S100×780/11 by Czylok Sp. z o.o., Jastrzębie Zdrój, Poland) in a nitrogen stream (5 dm<sup>3</sup>/min). The temperature in the furnace was increased at a rate of 10°C/min to an activation temperature of 800°C, which was maintained in the furnace for 2 h. After completion of the activation process, the samples were left in the reactor to reach room temperature. The material obtained was flooded with 5% HCl and left for 1 h. The sample was washed abundantly with hot distilled water until the chloride ions (Cl<sup>-</sup>) disappeared from the effluent and dried at 105°C. This sample was designated BC2. Fig. 1 shows the prepared samples.

Methylene blue (MB) was purchased from Acros Reagents Poland. Povidone-iodine (PVP-I) was purchased from Pol-Aura Chemical Reagents (Poland). These substances occur locally in surface waters, underground waters, raw and treated sewage, and even in drinking water [51,52]. Selected chemical properties of MB and PVP-I are presented in Table 1.

### 2.2. Instrumentation

The content of basic elemental components (C, H, N, S) was determined on a LECO Tru/Spec CHN/S elemental analyzer. The specific surface area and porosity were determined using nitrogen adsorption at 77 K on a micromeritics ASAP 2020 analyzer. The granulometric analysis was performed on an Analysette 22 NeXT analyzer by Fritsch. The pH of the water was determined by the potentiometric method using an Elmetron CP-401 pH meter. MB and PVP-I concentrations were quantified on a Hach-Lange DR5000 UV-VIS spectrophotometer with an operational range of 190–1,100 nm.

### 2.3. Physical and chemical analysis

Biochars were characterized in terms of their physical and chemical properties, such as: pH, moisture, ignition losses, ash content, total carbon content, specific surface area, porosity, the content of elements such as: C, H, N, S and O, and granulometric properties.

Moisture content ( $W_a$ ) in the tested samples was determined using the gravimetric method in accordance with the Polish standard PN-EN ISO 18134-2:2017-03 [54]. The measurement consisted in measuring the mass loss of a biochar weighing  $1 \pm 0.1$  g. The sample was placed in a laboratory dryer heated to  $105^\circ\text{C} \pm 5^\circ\text{C}$  for 90 min; after the sample had cooled down, the mass measurement was performed.

The ash content in the tested samples was determined in accordance with the PN-ISO 1171 standard [55].  $1 \pm 0.1$  g of biochar was weighed into a ceramic boat and placed in a furnace at a temperature of  $815^\circ\text{C} \pm 10^\circ\text{C}$  for 90 min. After the sample had cooled down, the mass measurement was performed. The ash content was expressed on a wet basis as follows:

$$A = \left( \frac{100 - W_a}{100} \right) \times A_a \quad (1)$$

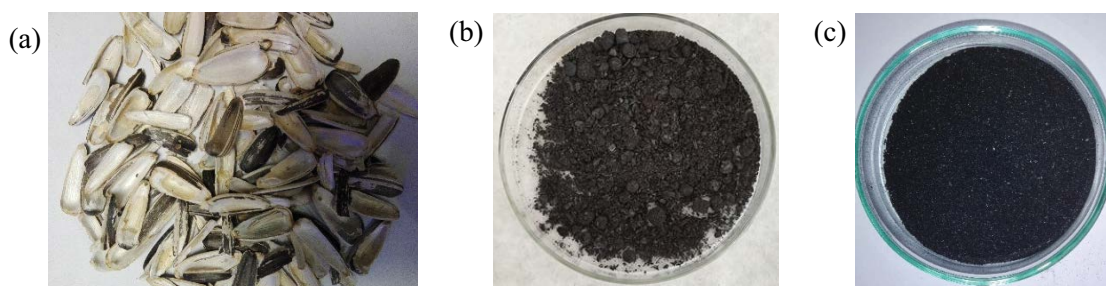
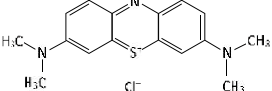
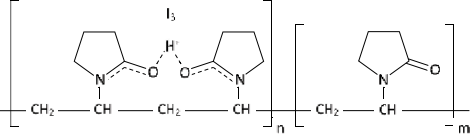


Fig. 1. View of the biomass used: (a) sunflower husks, (b) biochar obtained from the pyrolysis of sunflower husk (BC1) and (c) biochar obtained after chemical activation (BC2).

Table 1  
Chemical characterization of methylene blue and povidone-iodine (mostly based on [53])

Parameter	Methylene blue (MB)	Povidone-iodine (PVP-I)
Structure		
Formula	$C_{16}H_{18}ClN_3S$	$(C_6H_9NO)_k \cdot xI$
Molecular weight (g/mol)	319.85	Variable: $k \cdot 111.145 + x \cdot 126.90$
Partition coefficient*, $\log P_{ow}$	0.75	Not available
Dissociation constant, $pK_a$	3.14	Not available
Form in water solution	Cationic	Slowly transforming into cationic form while liberating iodine anions

\* $\log P_{ow}$  – the octanol-water partition coefficient expressed in logarithmic form.

where  $A$  (%) is the ash content in the sample on a wet basis;  $A_a$  (%) is the ash content in the analytical sample;  $W_a$  (%) is the moisture content in the analytical sample.

The fixed carbon (FC) content was calculated using the equation:

$$FC = 100 - VM - A \quad (2)$$

where FC (%) is the fixed carbon content in the sample on a dry basis; VM (%) and  $A$  (%) are the volatile matter and ash content of the sample, respectively, on a dry basis [56]. The determination of the content of volatile matter was carried out in accordance with the PN-EN ISO 18123:2016-01 standard [57]. When determining the volatile and non-combustible components (ash), the samples were calcined to a constant mass in a muffle furnace of the FCF22S type (CZYLOK, Poland).

The effectiveness of the modification process was estimated with the iodine value (IV) according to [58] as well as by specific surface area and pore volume analysis in liquid nitrogen.

The content of basic elemental components (C, H, N, S) was determined on a LECO Tru/Spec CHN/S elemental analyzer. Oxygen content was determined by calculation method based on the difference according to the following equation:

$$O = 100 - (A + C + N + H + S) \quad (3)$$

where O (%) – oxygen content; A (%) – ash content; C (%) – carbon content; N (%) – nitrogen content; H (%) – hydrogen content; S (%) – sulfur content.

In addition, the H/C and O/C ratios were determined. The H/C ratio, defining the hydrophobic character of the solid, and the O/C ratio, determining the presence of functional oxygen groups, were calculated from the elemental composition of biochar.

#### 2.4. Point of zero charge ( $pH_{pzc}$ )

The point of zero charge pH ( $pH_{pzc}$ ) is the pH value at which the surface of a solution or suspension of a solid in water has an electrical charge of zero. The measurement of

the surface neutralization point ( $pH_{pzc}$ ) of the adsorbent was determined using the constant addition method [59]. 50 mL of 0.01 M NaCl solution was prepared in glass bottles. The pH of the solution was then adjusted from 2 to 11 using solutions of 0.1 M HCl and 0.1 M NaOH. The bottles were sealed and left for 2 h. After this time, the initial pH of the solution was determined ( $pH_{initial}$ ), and then 0.15 g of biochar was added to each bottle. The bottles were purged with nitrogen gas to drive  $CO_2$  out of the solution and sealed. The samples were then shaken for 24 h and set aside. After 72 h of equilibration at room temperature, the pH of the solution was measured in each bottle, which was designated as  $pH_{final}$ . Based on the curve obtained from the difference of  $pH_{initial}$  and  $pH_{final}$  vs.  $pH_{initial}$ , the  $pH_{pzc}$  value was determined. At the  $pH_{pzc}$  value, the charge of the surface adsorbent is zero. The surface of the adsorbent does not induce the release of either  $H^+$  or  $OH^-$  ions, nor does it acquire a charge as a result of acid–base dissociation [60].

#### 2.5. Adsorption

BM or PVP-I of appropriate concentration, depending on particular stage of the studies, and volume of 0.1 dm<sup>3</sup> of distilled water were introduced into conical flasks. The flasks were shaken on a rotary shaker for 10 h at 20°C, and then placed in a dark room for 14 h. After this time, the water from the conical flasks was decanted and centrifuged in a centrifuge (MWP-2 type) at 2500 rpm.

MB and PVP-I concentrations were quantified on a UV-VIS spectrophotometer. MB absorbance was measured at the maximum absorption wavelength  $\lambda = 662$  nm and PVP-I at the wavelength  $\lambda = 210$  nm. The spectrophotometric method was also used by other researchers, for example, [43] for MB and [61] for PVP-I. Each measurement was performed 3 times and an average was taken.

The removal efficiency was calculated as follows:

$$E = \left( \frac{C_i - C_e}{C_i} \right) \times 100\% \quad (4)$$

where  $C_i$  and  $C_e$  are the initial and final equilibrium concentrations of MB or PVP-I, respectively. The adsorbed

mass of BM or PVP-I per unit of adsorbent mass was determined using the following equation:

$$q = \left( \frac{C_i - C_e}{m_a} \right) \times V \quad (5)$$

where  $m_a$  (g) is the adsorbent mass and  $V$  is the solution volume (0.1 dm<sup>3</sup>).

## 2.6. Adsorption optimization

The central composite design (CCD) for three variables with  $\alpha = 2^{(3/4)} \approx 1.68$  was used in the research to determine the optimal conditions for MB and PVP-I removal. The independent variables were: the initial concentration of MB and PVP-I ( $C_i$ ), adsorbent mass ( $m_a$ ) per solution volume (0.1 dm<sup>3</sup>), and the initial pH of the solution (pH<sub>i</sub>). The response variable was the removal efficiency ( $E$ ) given by Eq. (4). The ranges of the independent variables were 3–11 for pH<sub>i</sub>, 0.1–0.6 g for  $m_a$  at solution volume 0.1 dm<sup>3</sup>, and 30–250 mg/dm<sup>3</sup> for MB, 10–60 mg/dm<sup>3</sup> for PVP-I concentrations. The response (percentage removal efficiency  $E$ ) was approximated by a second-order polynomial with respect to normalized initial concentration, adsorbent mass and pH value (denoted as  $x_1$ ,  $x_2$  and  $x_3$ , respectively) as follows:

$$\begin{aligned} \tilde{E} = & a_0 + a_1x_1 + a_2x_2 + a_3x_3 + a_4x_1x_2 + a_5x_1x_3 \\ & + a_6x_2x_3 + a_7x_1^2 + a_8x_2^2 + a_9x_3^2 \end{aligned} \quad (6)$$

where  $\tilde{E}$  is the approximation of the removal efficiency, and  $a_0, a_1, \dots, a_9$  are coefficients to be determined by means of the least squares method using linear regression. In the analysis, all combinations of base functions 1,  $x_1, \dots, x_3^2$  were used to find the best approximation with respect to the adjusted  $R^2$ , which penalizes the count of terms. Then the approximation with the highest value of adjusted  $R^2$  was used for establishing the optimal conditions of adsorption.

## 2.7. Adsorption kinetics

The studies on MB and PVP-I adsorption kinetics were carried out with one-component aqueous solutions consisting of deionized water and the tested compound. The initial concentration of MB was 20 mg/dm<sup>3</sup>, the volume of the solution was 50 mL, to which 0.1 g of BC2 biochar was added. The kinetics studies for PVP-I were carried out under the same conditions, but for the initial concentration of PVP-I equal to 50 mg/dm<sup>3</sup>.

The following models were used for kinetic description: pseudo-first-order (PFO), pseudo-second-order (PSO), intraparticle diffusion (IPD) and particle diffusion with one term (PD1) [62]. If  $q_t$  represents the amount of adsorbed mass per adsorbent mass (in mg/g),  $t$  is time, and  $q_e$  the equilibrium value of  $q_t$  for  $t \rightarrow \infty$ , then PFO and PSO models are described with the following equations:

$$q_t^{\text{PFO}} = q_e \left( 1 - e^{-k_1 t} \right) \quad (7)$$

$$q_t^{\text{PSO}} = q_e \frac{q_e k_2 t}{1 + q_e k_2 t} \quad (8)$$

where  $k_1$  and  $k_2$  are constants related with adsorption rate. The times of half saturation in these models, when  $q_t = q_e/2$ , are as follows:

$$t_{\frac{1}{2}}^{\text{PFO}} = \frac{\ln 2}{k_1} \quad (9)$$

$$t_{\frac{1}{2}}^{\text{PSO}} = \frac{1}{k_2 q_e} \quad (10)$$

The diffusion model into a sphere of radius  $a$  is represented by the following equation:

$$q_t^{\text{PD}} = q_e \left( 1 - \frac{6}{\pi^2} \sum_{n=1}^{\infty} \frac{1}{n^2} \exp\left(-\frac{n^2 \pi^2 D t}{a^2}\right) \right) \quad (11)$$

where  $D$  is the transport coefficient. The series is often approximated with a square root of time as follows:

$$q_t^{\text{IPD}} = k_i \sqrt{t} + C_i \quad (12)$$

where  $k_i$  and  $C_i$  are constants, and the model is called the intraparticle diffusion (IPD) model. Another approximation for Eq. (11), applicable for large enough time, is obtained by taking only term with  $n = 1$  (the remaining terms are much weaker and vanish much quicker):

$$q_t^{\text{PD1}} \approx q_e \left( 1 - \frac{6}{\pi^2} \exp(-Bt) \right) \quad (13)$$

This model is denoted as PD1 (particle diffusion model with 1 term). Then:

$$t_{\frac{1}{2}}^{\text{PD1}} = \ln \left( \frac{12}{\pi^2} \right) \frac{1}{B} \quad (14)$$

The goodness of fitting of kinetics models was evaluated with use of standard error of regression.

$$S^{\text{model}} = \sqrt{\frac{1}{n-p-1} \sum_{i=1}^n (q_i - q_i^{\text{model}})^2} \quad (15)$$

where  $n$  is count of experimental points, and  $p$  is the number of parameters in the model.

## 2.8. Adsorption thermodynamics

In order to investigate the effect of temperature, sorption tests were carried out at temperatures of 20°C, 30°C, 40°C, 50°C and 60°C in the range of initial concentrations from 30 to 300 mg/dm<sup>3</sup> for MB and from 10 to 100 mg/dm<sup>3</sup> for PVP-I. The mass of the adsorbent was 0.4 g, and the volume of the solution was 0.1 dm<sup>3</sup>.

Then, thermodynamic parameters were determined: enthalpy change  $\Delta H$  (kJ/mol), entropy change  $\Delta S$  (kJ/(mol·K)) and Gibbs free energy change  $\Delta G$  (kJ/mol). According to the van't Hoff equation:

$$\ln K_{\text{eq}} = -\frac{\Delta H}{RT} + \frac{\Delta S}{R} \quad (16)$$

where  $K_{\text{eq}}$  is the equilibrium constant of the reaction,  $R$  is the universal gas constant (8.314 J/(mol·K)),  $T$  is temperature (K). The equilibrium constant was calculated as:

$$K_{\text{eq}} = \frac{K_L M_A C_r}{\gamma} \quad (17)$$

where  $K_L$  is Langmuir constant (dm<sup>3</sup>/mg),  $M_A$  is molar mass of adsorbate (g/mol),  $\gamma$  is activity coefficient (assumed equal to 1 due to high dilution of the solution), and  $C_r = 1$  mol/dm<sup>3</sup> is used to obtain dimensionless value  $K_{\text{eq}}$  [63]. The values of  $\Delta H$  and  $\Delta S$  were obtained from fitting the measurement points ( $T, K_{\text{eq}}$ ) in coordinates ( $1/T, \ln K_{\text{eq}}$ ) assuming a constant value of  $\Delta H$ . The Gibbs free energy change was determined as:

$$\Delta G = \Delta H - T\Delta S \quad (18)$$

### 3. Results and discussion

#### 3.1. Physical and chemical characteristics

The physical and chemical characteristics of sunflower husk biochar obtained in the pyrolysis process at 500°C (sample BC1) and after its chemical activation at 800°C (sample BC2) are presented in Tables 2–4. The obtained results indicate an influence of chemical activation on physical and chemical properties of the biochar. Both BC1 and BC2 samples are characterized by a high pH value of 8.9 and 9.6, respectively. The basic nature of biochars is associated with the pyrolysis process, under the influence of which carbonates are formed and aromatic structures with condensed rings with C–O bonds or reduction of carboxyl groups occur [64–66]. The alkalinity of biochars is caused by negatively charged organic groups such as COO (carboxylate), OH (hydroxyl) and carbonates bound to the surface of biochars. As the pyrolysis temperature increases, the number of acidic functional groups decreases, which is correlated with the loss of volatile substances (Table 2) [67]. The obtained values of mineral parts (ash) in the biochars were similar and amounted to about 7%. Ash content in sunflower husk biochar was similar to that obtained in other works, for example, 8.13% for corn husk biochar (pyrolysis at 600°C) [68], 7.85% for apple branches biochar (pyrolysis at 400°C) [69], or 9.5% for bamboo biochar

(pyrolysis at 500°C) [70]. Biochars with lower ash content generally have higher porosity [71], which finds confirmation in Table 3. Chemical activation and high pyrolysis temperature caused a large increase in specific surface area, micropore and mesopore volume. The biochar BC2 has a larger pore space compared to BC1, because higher temperature causes additional evaporation of volatile components in biomass [71,72], and the chemical activation induces changes in the surface structure. The lower content of volatile components and the higher content of carbon bound to the solid matter (FC) in the BC2 biochar (Table 2) prove that almost all lignocellulosic material contained in the raw material was decomposed during chemical activation at 800°C [68,73]. The increase in the pyrolysis temperature and chemical activation caused and increase in the total FC content by about 6.5%. The results show also that the volatiles in BC1 sample were not completely evaporated, which may be the reason for blocking some pores. This is confirmed by a rather low available surface area indicated by the iodine value of 92 mg/g and specific surface area of 32.5 m<sup>2</sup>/g. In contrast, the determined iodine value of 495 mg/g and specific surface area of 740.5 m<sup>2</sup>/g for BC2 biochar indicates a higher sorption capacity of this biochar and suggests the possibility of using it as a much better sorbent than BC1 biochar.

The elemental analysis of the biochar showed a loss of hydrogen and oxygen and the enrichment of the material with carbon after the chemical activation at 800°C (Table 4). The C content increased from 75.2% to 83.5%, while the H

Table 3  
Structural characterization of biochar samples BC1 and BC2

Parameter	BC1	BC2
Specific surface area (m <sup>2</sup> /g)	32.5	740.5
Total pore volume (cm <sup>3</sup> /g)	0.0183	0.279
t-Plot micropore volume (cm <sup>3</sup> /g)	0.0105	0.242
BJH desorption cumulative volume of pores 1.7–50 nm (cm <sup>3</sup> /g)	0.00572	0.0419
BJH desorption cumulative surface area of pores 1.7–50 nm (m <sup>2</sup> /g)	0.901	51.96
BJH desorption dominant mesopore width (nm)	10–20	4
Density (g/cm <sup>3</sup> )	0.40	0.46

Table 4  
Elemental composition of the tested biochars

Biochar	BC1	BC2
C (%)	75.2	83.5
H (%)	2.4	0.97
N (%)	1.033	0.869
S (%)	0.045	0.06
O (%)	21.3	14.6
H/C	0.03	0.01
O/C	0.28	0.18

Table 2  
Physical and chemical characteristics of the tested biochars

Biochar	BC1	BC2
pH <sub>H2O</sub>	8.9	9.6
Moisture, $W_a$ (%)	0.3	0.2
Fixed carbon, FC (%)	81.2	87.8
Ash, A (%)	7.3	7.0
Volatile matter, VM (%)	11.5	5.2
Iodine value, IV (mg/g)	92	495

and O contents decreased from 2.4% to 0.97% and from 21.3% to 14.6%, respectively, with an increase in temperature from 500°C to 800°C. According to literature reports, it is most likely that higher temperatures of pyrolysis lead to the decomposition of oxygen bonds and the release of low-molecular by-products containing H and O [74]. Similarly, the nitrogen content also decreased. The knowledge of H/C ratio (degree of aromaticity) and O/C ratio (degree of polarity) allows to conclude about the diversity of the chemical structure of biochars. The H/C and O/C ratios of the tested biochars fall in the range of 0.01–0.03 and 0.28–0.18, respectively. The ratios decreased with increasing pyrolysis temperature. These results are consistent with previous studies [68,69]. The O/C ratio, which decreases with the activation temperature, suggests that the surface of the organic material is more hydrophobic and less hydrophilic [69]. In addition, the H/C and O/C ratios indicate the loss of functional groups containing O and H (such as: carboxyl, hydroxyl and others), and greater degree of carbonization.

The above properties indicate that BC2 sample should be a better adsorbent than BC1. Therefore, further research was focused on BC2 sample. The analysis of the granulometric composition of BC2 (Fig. 2) indicates the presence of four dominant grain classes in the tested material: 1–0.03 mm, 0.031–0.05 mm; 0.051–0.1 mm and 0.101–0.35 mm. The percentage share of these classes in the total amount of waste is respectively: 21.4%, 8.6%, 19% and 51%. The dominant grain class in the tested sample is the fraction >0.05 mm, which in total accounts for about 70%.

### 3.2. Point of zero charge pH

The  $\text{pH}_{\text{pzc}}$  of an adsorbent is the pH of a solution containing this adsorbent when the net surface charge is zero [75]. At the pH values lower than  $\text{pH}_{\text{pzc}}$ , the surface of adsorbent is positively charged. The surface charge of adsorbent is negative at the pH values higher than  $\text{pH}_{\text{pzc}}$  [76]. Fig. 3 shows the  $\text{pH}_{\text{pzc}}$  results for the tested biochar BC2. The  $\text{pH}_{\text{pzc}}$  of the adsorbent is 8.4. Since MB is a cationic dye, and PVP-I slowly takes cationic form while gradually liberating iodine

anions, both adsorbates should be adsorbed with higher efficiency at pH larger than 8.4.

### 3.3. Adsorption optimization

The input and output data for adsorption optimization on BC2 with use of CCD are presented in Table 5. The removal efficiency of MB is high and falls in the range 86%–100%. As for PVP-I, the efficiency is much lower and varies from around 5% to 75%. The parameters of the approximation of the removal efficiency [Eq. (6)] are shown in Table 6, and the resulting approximations are illustrated in Fig. 4. The details can be found in supporting information.

It follows that pH insignificantly affects the removal efficiency of PVP-I – in both cases the influence of pH is statistically insignificant (all coefficients of terms involving  $x_3$  are absent). This suggests that the adsorption mechanism is weakly related with electrostatic interactions between the adsorbent surface and the adsorbate particles, and indicates other mechanism of adsorption. Various mechanisms of adsorption of MB on a biochar was also reported in [77]. The fitting functions can be presented in  $(C, m_e)$  coordinates (Fig. 4). In case of MB, the removal efficiency has a maximum

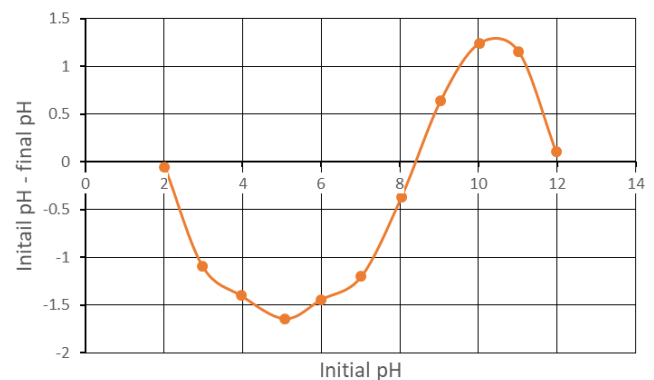


Fig. 3. Point of zero charge pH for the tested biochar.

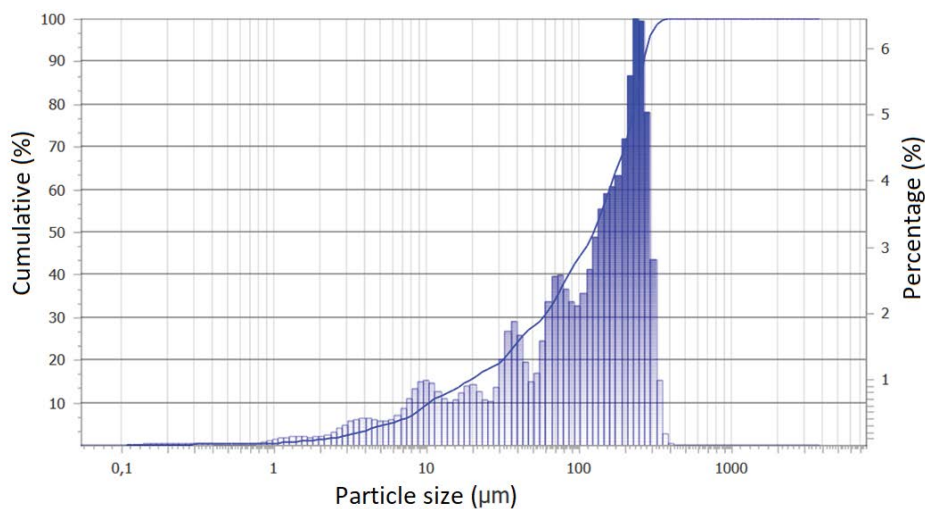


Fig. 2. Granulometric analysis of the BC2 biochar.

Table 5  
Input and output data for removal optimization with central composite design

$x_1$	$C_i$ (mg/dm <sup>3</sup> )		$x_2$	$m_a$ (g)	$x_3$	pH	$C_e$ (mg/dm <sup>3</sup> )		Efficiency (%)	
	MB	PVP-I					MB	PVP-I	MB	PVP-I
-1	75	20	-1	0.2	-1	4.6	2.9	15.3	96.1	23.5
1	205	50	-1	0.2	-1	4.6	20.8	40.4	89.8	19.2
-1	75	20	1	0.5	-1	4.6	0.19	12.9	99.8	35.5
1	205	50	1	0.5	-1	4.6	8.9	30.2	95.7	39.6
-1	75	20	-1	0.2	1	9.4	3.0	14.9	96.0	25.5
1	205	50	-1	0.2	1	9.4	20.7	38.8	89.9	22.4
-1	75	20	1	0.5	1	9.4	0.28	10.3	99.6	48.5
1	205	50	1	0.5	1	9.4	10.4	35.5	94.9	29.0
0	140	35	0	0.35	0	7	7.8	32.7	94.4	6.6
0	140	35	0	0.35	0	7	5.6	29.1	96.0	16.9
0	140	35	0	0.35	0	7	4.8	32.2	96.5	8.0
-1.68	30	10	0	0.35	0	7	0.19	2.5	99.4	75.0
1.68	250	60	0	0.35	0	7	20.0	47.1	92.0	21.5
0	140	35	-1.68	0.1	0	7	20.1	32.6	85.7	6.9
0	140	35	1.68	0.6	0	7	18.1	27.7	87.1	20.9
0	140	35	0	0.35	-1.68	3	7.2	28.1	94.9	19.7
0	140	35	0	0.35	1.68	11	6.9	33.2	95.1	5.1
0	140	35	0	0.35	0	7	6.1	29.5	95.7	15.7
0	140	35	0	0.35	0	7	5.9	30.2	95.8	13.7
0	140	35	0	0.35	0	7	6.0	31.7	95.7	9.4

Table 6  
Best fit parameters for removal efficiency given by Eq. (6)

Methylene blue (MB)			Povidone-iodine (PVP-I)		
Coefficient	Value	Standard error	Coefficient	Value	Standard error
$a_0$	95.9	0.62	$a_0$	13.8	2.4
$a_1$	-2.45	0.49	$a_1$	-8.26	2.2
$a_2$	1.50	0.49	$a_2$	6.26	2.2
$a_7$	0.61	0.47	$a_7$	13.6	2.2
$a_8$	-2.68	0.47			
Adjusted $R^2 = 0.77$			Adjusted $R^2 = 0.75$		

corresponding to adsorbent mass around 0.4 g (per 0.1 dm<sup>3</sup>). As for PVP-I, the maximum occurs for largest considered adsorbent mass 0.6 g (per 0.1 dm<sup>3</sup>). As a result, such adsorbent masses were used in further research.

### 3.4. Adsorption kinetics

The adsorption kinetics of MB and PVP-I on BC2 biochar is illustrated in Fig. 5 and Table 7. The adsorption rate is higher for MB – 90% of the equilibrium value is achieved after around 2 min. As for PVP-I, the adsorption rate is visibly slower. The course of the MB kinetic curve indicates strong interactions between the active sites present on the biochar surface and the MB molecules. The rapid course of the adsorption process in the initial stage is associated with

a large number of available active sites on the surface of the adsorbent capable of adsorbing dye molecules. However, in the case of PVP-I sorption, the curve shows that particles of this compound gradually occupied the surface of the adsorbent. With the passage of time, the active sites on the surface of BC2 were completely saturated with adsorbate, both for MB and PVP-I, and the experimental curves reached saturation (Fig. 5). The analysis of the curves shows that about 60 min is sufficient to establish the adsorption equilibrium on the tested adsorbent. The obtained equilibrium time is comparable to those reported in the literature, such as for MB adsorption on biochar obtained from the pyrolysis of barley malt pomace [78].

The course of the curves presented in Fig. 5 also indicates a slightly different mechanism of establishing the equilibrium for MB and PVP-I sorption. The adsorption kinetics was modelled by 4 theoretical models: PFO, PSO, IPD and PD1. The quality of fit for the PFO and PSO models is similar and clearly much higher than that for IPD and PD1. The three models also yield similar  $q_e$  values. However, the PSO model obtained the lowest standard error of regression ( $S = 0.02$  mg/g) compared to the PFO ( $S = 0.14$  mg/g) model for MB sorption. This model is explained by external diffusion in the boundary film, surface adsorption and intramolecular diffusion processes [79]. According to [80], the PSO model indicates that chemisorption determines the rate of the MB adsorption process, and the adsorption capacity is proportional to the active areas. As for PVP-I, the experimental data was best reflected by the PSO model ( $S = 0.20$  mg/g), which suggests that PVP-I adsorption also depends on the adsorbate and includes the process of chemisorption



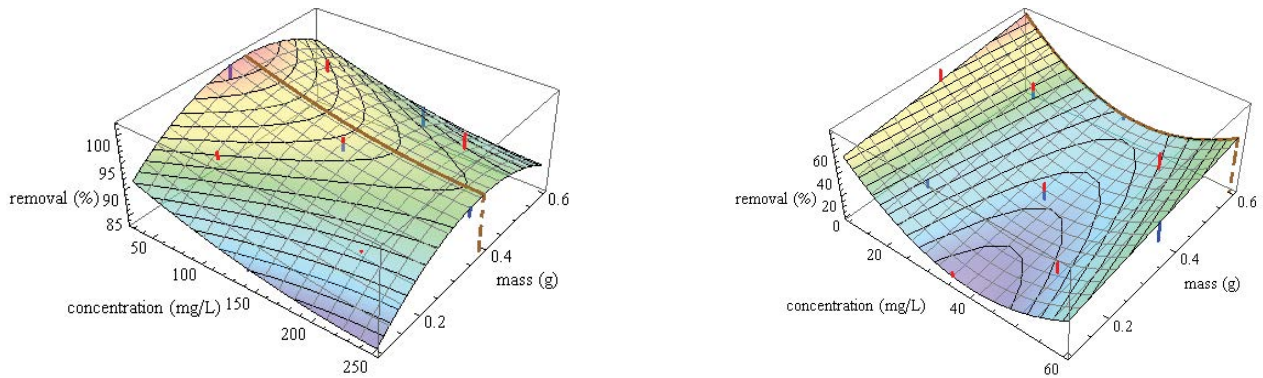


Fig. 4. Removal efficiency vs. initial concentration and adsorbent mass for MB (a) and PVP-I (b); red and blue lines correspond to differences between experiment and approximation (red – positive, blue – negative); brown line indicates the maximum efficiency for a given initial concentration.

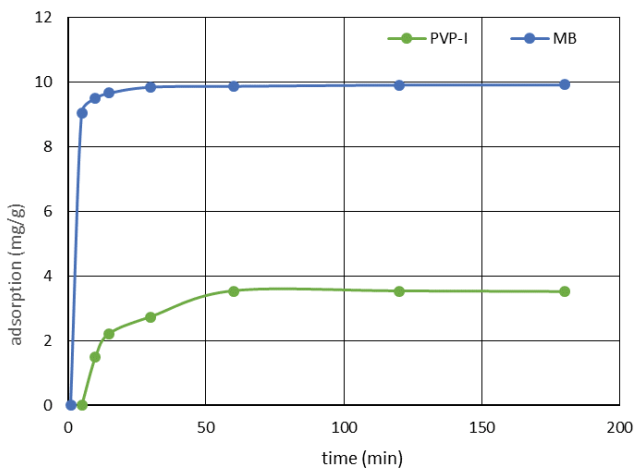


Fig. 5. Kinetics of MB and PVP-I adsorption on BC2 biochar for initial concentration of MB and PVP-I equal to 20 and 50 mg/dm<sup>3</sup>, respectively.

and physisorption. Similar kinetic model fittings were reported for many different pollutant-adsorbent systems in literature [81,82].

In addition, large differences were observed between the adsorption rate constants for MB and PVP-I. For MB sorption, the half-saturation times predicted by the models range from 25 to 80 s, and for PVP-I they were much greater and ranged from 7 to 16 min (Table 7). Such large differences were probably due to the fact that the PVP-I particles are much larger than the MB particles ( $1.43 \times 0.72$  nm), as a result of which the MB particles could enter smaller pores on the biochar surface easier than the PVP-I particles [83].

### 3.5. Thermodynamic studies

The thermodynamic studies require knowledge on the molar mass of the adsorbate. In case of MB the molar mass is well established, but for PVP-I it is not. Therefore, the calculations for PVP-I were performed for various molar masses equal to the  $\alpha 364.95$ , where 364.95 is the molar mass of the fundamental PVP-I structure (monomer

Table 7

Parameters related with kinetics models for MB and PVP-I adsorption

Parameter/ Indicator	Unit	MB	PVP-I
		$C_0 = 20 \text{ mg/dm}^3$	$C_0 = 50 \text{ mg/dm}^3$
PFO, Eqs. (7) and (9)			
$q_e$	mg/g	9.79	3.69
$k_1$	1/min	0.50	0.05
$t_{1/2}$	min	1.38	13.22
$S$	mg/g	0.14	0.32
PSO, Eqs. (8) and (10)			
$q_e$	mg/g	9.96	4.22
$k_2$	g/(mg·min)	0.20	0.015
$t_{1/2}$	min	0.5	15.75
$S$	mg/g	0.02	0.20
IPD, Eq. (12)			
$k_i$	mg/(g·√min)	0.43	0.28
$C_i$	mg/g	5.94	0.70
$S$	mg/g	3.03	0.48
PD1, Eqs. (13) and (14)			
$q_e$	mg/g	9.54	3.59
$B$	1/min	0.49	0.03
$t_{1/2}$	min	0.40	7.00
$S$	mg/g	1.55	0.70

plus two atoms of iodine), and  $\alpha \geq 1$  is a multiplier. Then Eqs. (16)–(18) yield:

$$\Delta S(\alpha) = \Delta S(1) + R \ln \alpha \quad (19)$$

$$\Delta G(\alpha) = \Delta G(1) - RT \ln \alpha \quad (20)$$

where  $\Delta S$  and  $\Delta G$  are functions of  $\alpha$ . Therefore, the larger the PVP-I complex the larger  $\Delta S$  and the smaller  $\Delta G$ , whereas  $\Delta H$  is not affected by size of PVP-I complex.

Fig. 6 shows the plot  $\ln K_{eq}$  vs.  $1/T$ , and Table 8 summarizes the results of the analysis. The Gibbs free energy change is negative for both adsorbates, which means that sorption occurs spontaneously. With increasing temperature, adsorption increased in the case of PVP-I, which means that higher temperatures favor the adsorption of PVP-I, but do not affect significantly the adsorption of MB (Fig. 6). This is also confirmed by the determined value of the enthalpy change close to zero – in the considered temperature range, the temperature change had little effect on the MB sorption process. However, in the case of PVP-I, the enthalpy change is clearly positive. This means that the sorption of PVP-I on biochar from sunflower husks is an endothermic process, better occurring at higher temperatures. Small positive values of  $\Delta S$  indicate an increase in the degree of randomness (or disorder) in the solid/solution during the sorption of MB and PVP-I [77]. The effect of variable molar mass of PVP-I does not affect significantly the results (see the last two columns of Table 8).

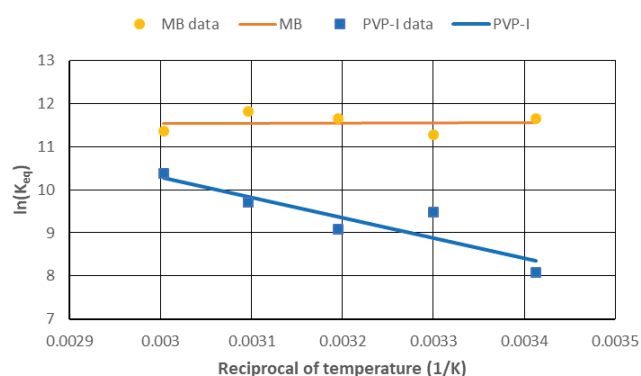


Fig. 6. Results of studies on thermodynamics of MB and PVP-I sorption on BC2.

Known values of enthalpy change  $\Delta H$  and Gibbs free energy change  $\Delta G$  also allow to characterize the adsorption process as physical or chemical. When  $\Delta H$  is less than 40 kJ/mol, Van der Waals forces act between the adsorbate and the adsorbent surface, which corresponds to the physical adsorption process. When  $\Delta H$  is in the range of 40–200 kJ/mol, the acting force is a chemical bond and can be attributed to chemical adsorption [84]. In the conducted tests,  $\Delta H$  for PVP-I sorption was 39.4 kJ/mol, and only  $-0.2$  kJ/mol for MB. The value of  $\Delta H$  for PVP-I is close to the cut-off value between physical sorption and chemisorption, which is in line with the sorption kinetics of PVP-I, where it was found that adsorption includes, apart from chemisorption, also physical sorption (section 3.4).

### 3.6. Comparative studies

Based on Table 5 the adsorbent amount of adsorbate per unit mass of adsorbent was calculated. The maximum value equals 120 and 5.6 mg/g for MB and PVP-I, respectively. The properties of the biochar represented by BC2 sample were compared with those reported in literature (Table 9). It follows that the maximum sorption capacity of the tested biochar with respect to MB is comparable with

Table 8  
Thermodynamic parameters of MB and PVP-I sorption on prepared sunflower husks

Parameter	MB	PVP-I for $\alpha = 1$	PVP-I for $\alpha = 30$
$\Delta H$ , kJ/mol	$-0.2 \pm 6.5$	$39.4 \pm 10.9$	$39.4 \pm 10.9$
$\Delta G$ , kJ/mol	$-32.0$ to $-28.1 \pm 13.5$	$-28.5$ to $-20.3 \pm 22.5$	$-37.9$ to $-28.6 \pm 22.5$
$\Delta S$ , kJ/(mol·K)	$0.1 \pm 0.02$	$0.20 \pm 0.03$	$0.23 \pm 0.03$

Table 9  
Comparison of the maximum adsorption capacity of the obtained biochar with other biochars

Biomass	Activation method	Adsorbate	Maximum sorption capacity (mg/g)	References
Sunflower husks	Pyrolysis at 800°C plus activation with $K_2CO_3$	MB PVP-I	120 5.6	This study
<i>Cedrela odorata</i> L	Pyrolysis at 400°C	MB	158.8	[85]
Banana pseudostem	Pyrolysis at 200°C plus modification with phosphomolybdic acid	MB	87.28 146.23	[86]
Areca catechu nuts	Pyrolysis at 400°C plus activation with $H_3PO_4$	MB	333.3	[43]
White pine wood (80%), spruce i fir (20%)	Pyrolysis up to 525°C	MB	3.99	[87]
Solid fraction of pig slurry	Pyrolysis at 400°C	MB	16.3	[87]
Cardboard waste	Pyrolysis at 500°C	MB	1.66	[87]
Olive pits	Pyrolysis at 500°C	Triclosan (PPCP)	12	[88]
Olive tree waste	Pyrolysis at 300°C	Triclosan (PPCP)	8.5	[88]
Waste mix of various pruned trees	Pyrolysis at 900°C	Triclosan (PPCP)	4.5	[88]
Empty palm bunch	Pyrolysis at 450°C plus activation with $H_2SO_4$	Triclosan (PPCP)	35.4	[89]

that of other biochars. Unfortunately, no information on PVP-I adsorption on biochars was encountered in literature, although it was very extensively used during COVID-19 epidemic. Therefore, other antiseptic substance (triclosan) was included into the comparison.

#### 4. Conclusions

Based on the results obtained the following conclusions concerning the adsorption of MB and PVP-I on BC2 can be formulated:

- In the tested ranges of values of adsorption conditions the MB and PVP-I adsorption was best for adsorbent dose equal to 4 and 6 g/dm<sup>3</sup>, respectively.
- The removal efficiency was statistically independent on the pH of the solution in the tested range 3 to 11.
- The results of kinetics studies indicate that the adsorption process for MB proceeds very quickly – after just a few minutes the adsorbent is practically saturated. However, in the case of PVP-I, the adsorption process is much slower and requires several dozen minutes. The kinetics is quite well described by the pseudo-second-order model, which indicates that adsorption involves chemical reactions in addition to physical sorption.
- Negative Gibbs free energy change indicates that adsorption is spontaneous and thermodynamically favored.
- The biochar obtained from sunflower husks in the pyrolysis process and chemical activation is an efficient, cheap and environmentally friendly adsorption material that can be used to remove MB and PVP-I from water and wastewater.

#### Funding

This research was financially supported by the Faculty of Infrastructure and Environment of the Czestochowa University of Technology.

#### References

- [1] X. Xu, H. Yang, C. Li, Theoretical model and actual characteristics of air pollution affecting health cost: a review, *Int. J. Environ. Res. Public Health*, 19 (2022) 3532, doi: 10.3390/ijerph19063532.
- [2] European Environment Agency, Report: The European Environment – State and Outlook 2020: Knowledge for Transition to a Sustainable Europe, 2019. Available at: <https://www.eea.europa.eu/soer/2020> (Access date 4.10.2022).
- [3] K. Zhang, R. Ruan, Z. Zhang, S. Zhi, An exhaustive investigation on antibiotics contamination from livestock farms within sensitive reservoir water area: spatial density, source apportionment and risk assessment, *Sci. Total Environ.*, 847 (2022) 157688, doi: 10.1016/j.scitotenv.2022.157688.
- [4] N. Kornak, J. Kostecka, Elements of the social perception of the economy of expired drugs, *Pol. J. Sustain. Dev.*, 23 (2019) 37–46 (in Polish).
- [5] D. Ginter-Kramarczyk, I. Kruszelnicka, Color problem in water (dye contamination), *Wodociągi - Kanalizacja*, 12 (2020) 24–27 (in Polish).
- [6] A. Koszowska, M. Ebisz, T. Krzyśko-Lupicka, Presence of pharmaceuticals and cosmetics in the aquatic environment as a new environmental health problem, *Medycyna Środowiskowa – Environ. Med.*, 18 (2015) 62–69 (in Polish).
- [7] A. Grdulska, R. Kowalik, Pharmaceuticals in water and wastewater – overview, *Struct. Environ.*, 12 (2020) 79–84, doi: 10.30540/sae-2020-009.
- [8] I.A. Al-Baldawi, A.A. Mohammed, Z.H. Mutar, S.R.S. Abdullah, S.S. Jasim, A.F. Almansoori, N.I. Ismail, Application of phytotechnology in alleviating pharmaceuticals and personal care products (PPCPs) in wastewater: source, impacts, treatment, mechanisms, fate, and SWOT analysis, *J. Cleaner Prod.*, 319 (2021) 128584, doi: 10.1016/j.jclepro.2021.128584.
- [9] Y.Y. Yang, J.L. Zhao, Y.S. Liu, W.R. Liu, Q.Q. Zhang, L. Yao, G.G. Ying, Pharmaceuticals and personal care products (PPCPs) and artificial sweeteners (ASs) in surface and ground waters and their application as indication of wastewater contamination, *Sci. Total Environ.*, 616–617 (2018) 816–823.
- [10] M. Liu, H. Yin, Q. Wu, Occurrence and health risk assessment of pharmaceutical and personal care products (PPCPs) in tap water of Shanghai, *Ecotoxicol. Environ. Saf.*, 183 (2019) 109497, doi: 10.1016/j.ecoenv.2019.109497.
- [11] S. Dey, F. Bano, A. Malik, Pharmaceuticals and Personal Care Product (PPCP) Contamination – A Global Discharge Inventory, M.N.V. Prasad, M. Vithanage, A. Kapley, Eds., *Pharmaceuticals and Personal Care Products: Waste Management and Treatment Technology*, Butterworth-Heinemann, 2019, pp. 1–26. Available at: <https://doi.org/10.1016/B978-0-12-816189-0.00001-9>
- [12] Y. Wang, Y. Wu, Q. Wang, J. Zhu, W. Shi, Z. Han, Y. Zhang, K. Chen, Virucidal effect of povidone-iodine against SARS-CoV-2 *in vitro*, *J. Int. Med. Res.*, 49 (2021), doi: 10.1177/03000605211063695.
- [13] S.H.S. Naqvi, M.J. Citardi, D. Cattano, L. Ostrosky-Zeichner, M.I. Knackstedt, R.J. Karni, Povidone-iodine solution as SARS-CoV-2 prophylaxis for procedures of the upper aerodigestive tract: a theoretical framework, *J. Otolaryngol. – Head & Neck Surg.*, 49 (2020), doi: 10.1186/s40463-020-00474-x.
- [14] G. Gandhi, L. Thimmappa, N. Upadhy, S. Carnelio, Could mouth rinses be an adjuvant in the treatment of SARS-CoV-2 patients? An appraisal with a systematic review, *Int. J. Dent. Hyg.*, 20 (2022) 136–144.
- [15] R. Kawana, T. Kitamura, O. Nakagomi, I. Matsumoto, M. Arita, N. Yoshihara, K. Yanagi, A. Yamada, O. Morita, Y. Yoshida, Y. Furuya, S. Chiba, Inactivation of human viruses by povidone-iodine in comparison with other antiseptics, *Dermatology*, 195 (1997) 29–35.
- [16] S. Tsuda, S. Soutome, S. Hayashida, M. Funahara, S. Yanamoto, M. Umeda, Topical povidone-iodine inhibits bacterial growth in the oral cavity of patients on mechanical ventilation: a randomized controlled study, *BMC Oral Health*, 20 (2020), doi: 10.1186/s12903-020-1043-7.
- [17] M. Eggers, T. Koburger-Janssen, M. Eickmann, J. Zorn, *In-vitro* bactericidal and virucidal efficacy of Povidone-iodine gargle/mouthwash against respiratory and Oral tract pathogens, *Infect. Dis. Ther.*, 7 (2018) 249–259.
- [18] B. Gao, Z. Wang, Q. Liu, R. Du, Immobilization of povidone-iodine on surfaces of silica gel particles and bactericidal property, *Colloids Surf., B*, 79 (2010) 446–451.
- [19] N.S.K. Nawalage, B.K.A. Bellanthudawa, Synthetic polymers in personal care and cosmetics products (PCCPs) as a source of microplastic (MP) pollution, *Mar. Pollut. Bull.*, 182 (2022) 113927, doi: 10.1016/j.marpolbul.2022.113927.
- [20] K. Lakkhal, J. Faidherbe, R. Choukhi, E. Boissier, X. Capdevila, Povidone-iodine: Features of critical systemic absorption, *Annales Françaises d'Anesthésie et de Réanimation*, 30 (2011) e1–e3, doi: 10.1016/j.annfar.2011.04.002.
- [21] M.K. Mouden, J. Labaye, D. Sarret, G. Cazajous, M. Herody, F. Didelot, Acute renal failure following internal administration of povidone-iodine: a case report, *Rev. Med. Int.*, 28 (2007) 556–558.
- [22] C.S. Kim, S.S. Kim, E.H. Bae, S.K. Ma, S.W. Kim, Acute kidney injury due to povidone-iodine ingestion, *Medicine*, 96 (2017) e8879, doi: 10.1097/MD.00000000000008879.
- [23] S. Vats, S. Srivastava, N. Maurya, S. Saxena, B. Mudgil, S. Yadav, R. Chandra, Advances in Dye Contamination: Health Hazards, Biodegradation, and Bioremediation, S. Kumar, M.Z. Hashmi, Eds., *Biological Approaches to Controlling Pollutants*,

- Advances in Pollution Research, Woodhead Publishing, 2022, pp. 139–162, doi: 10.1016/B978-0-12-824316-9.00020-3.
- [24] L. Young, J. Yu, Ligninase-catalyzed decolorization of synthetic dyes, *Water Res.*, 31 (1997) 1187–1193.
- [25] L. Lian, L. Guo, C. Guo, Adsorption of Congo red from aqueous solutions onto Ca-bentonite, *J. Hazard. Mater.*, 161 (2009) 126–131.
- [26] M. Czubaszek, J. Choma, Adsorption of selected dyes from aqueous solutions on nanoporous carbon materials obtained from polymer precursors, *Ochrona Środowiska*, 39 (2017) 3–8 (in Polish).
- [27] F. Meinck, H. Stooff, M. Kohlschutter, *Industrial Sewage. Toxic Effects of Substances Contained in Sewage on Plants and Animals*, Arkady, Warszawa, 1975 (in Polish).
- [28] M.A. Hassaan, A.E. Nemr, Health and environmental impacts of dyes: mini review, *Am. J. Environ. Sci. Eng.*, 3 (2017) 64–67.
- [29] T. Aysu, M.M. Küçük, Removal of crystal violet and methylene blue from aqueous solutions by activated carbon prepared from *Ferula orientalis*, *Int. J. Environ. Sci. Technol.*, 12 (2015), 2273–2284.
- [30] O. Üner, Ü. Geçgel, Y. Bayrak, Adsorption of methylene blue by an efficient activated carbon prepared from *Citrullus lanatus* rind: kinetic, isotherm, thermodynamic, and mechanism analysis, *Water Air Soil Pollut.*, 227 (2016) 247, doi: 10.1007/s11270-016-2949-1.
- [31] M. Behera, J. Nayak, S. Banerjee, S. Chakraborty, S.K. Tripathy, A review on the treatment of textile industry waste effluents towards the development of efficient mitigation strategy: an integrated system design approach, *J. Environ. Chem. Eng.*, 9 (2021) 105277, doi: 10.1016/j.jece.2021.105277.
- [32] Z. Talebzadeh, M. Masjedi-Arani, O. Amiri, M. Salavati-Niasari,  $\text{La}_2\text{Sn}_2\text{O}_7/\text{g-C}_3\text{N}_4$  nanocomposites: rapid and green sonochemical fabrication and photo-degradation performance for removal of dye contaminations, *Ultrason. Sonochem.*, 77 (2021) 105678, doi: 10.1016/j.ulsonch.2021.105678.
- [33] Y. Luo, G. Huang, Y. Li, Y. Yao, J. Huang, P. Zhang, S. Ren, J. Shen, Z. Zhang, Removal of pharmaceutical and personal care products (PPCPs) by MOF-derived carbons: a review, *Sci. Total Environ.*, 857 (2023) 159279, doi: 10.1016/j.scitotenv.2022.159279.
- [34] A. Demirbas, Agricultural based activated carbons for the removal of dyes from aqueous solutions: a review, *J. Hazard. Mater.*, 167 (2009) 1–9.
- [35] S. Samsami, M. Mohamadizani, M.H. Sarrafzadeh, E.R. Rene, M. Firoozbahr, Recent advances in the treatment of dye-containing wastewater from textile industries: overview and perspectives, *Process Saf. Environ. Prot.*, 143 (2020) 138–163.
- [36] A.K. Sahoo, A. Dahiya, B.K. Patel, *Biological Methods for Textile Dyes Removal From Wastewaters*, M.P. Shah, S. Rodriguez-Couto, R.T. Kapoor, Eds., Development in Wastewater Treatment Research and Processes, Elsevier, 2022, pp. 127–151.
- [37] H. Xiang, G. Ren, X. Yang, D. Xu, Z. Zhang, X. Wang, A low-cost solvent-free method to synthesize  $\alpha\text{-Fe}_2\text{O}_3$  nanoparticles with applications to degrade methyl orange in photo-Fenton system, *Ecotoxicol. Environ. Saf.*, 200 (2020) 110744, doi: 10.1016/j.ecoenv.2020.110744.
- [38] E. Ayranci, O. Duman, *In-situ* UV-Visible spectroscopic study on the adsorption of some dyes onto activated carbon cloth, *Sep. Sci. Technol.*, 44 (2009) 3735–3752.
- [39] O. Duman, S. Tunç, T.G. Polat, B.K. Bozoğlan, Synthesis of magnetic oxidized multiwalled carbon nanotube- $\kappa$ -carrageenan- $\text{Fe}_3\text{O}_4$  nanocomposite adsorbent and its application in cationic methylene blue dye adsorption, *Carbohydr. Polym.*, 147 (2016) 79–88.
- [40] O. Duman, S. Tunç, B.K. Bozoğlan, T.G. Polat, Removal of triphenylmethane and reactive azo dyes from aqueous solution by magnetic carbon nanotube- $\kappa$ -carrageenan- $\text{Fe}_3\text{O}_4$  nanocomposite, *J. Alloys Compd.*, 687 (2016) 370–383.
- [41] B. Mao, B. Sidhureddy, A.R. Thirupathi, P.C. Wood, A. Chen, Efficient dye removal and separation based on graphene oxide nanomaterials, *New J. Chem.*, 44 (2020) 4519–4528.
- [42] O. Duman, S. Tunç, T.G. Polat, Determination of adsorptive properties of expanded vermiculite for the removal of C.I. Basic Red 9 from aqueous solution: kinetic, isotherm and thermodynamic studies, *Appl. Clay Sci.*, 109–110 (2015) 22–32.
- [43] S. Joshi, R.G. Shrestha, R.R. Pradhananga, K. Ariga, L.K. Shrestha, High surface area nanoporous activated carbons materials from areca catechu nut with excellent iodine and methylene blue adsorption, *C*, 8 (2022) 2, doi: 10.3390/c8010002.
- [44] S. Meyer, B. Glaser, P. Quicker, Technical, economical, and climate-related aspects of biochar production technologies: a literature review, *Environ. Sci. Technol.*, 45 (2011) 9473–9483.
- [45] X. Wang, Z. Guo, Z. Hu, J. Zhang, Recent advances in biochar application for water and wastewater treatment: a review, *PeerJ*, 8 (2020) e9164, doi: 10.7717/peerj.9164.
- [46] K.N. Palansooriya, Y. Yang, Y.F. Tsang, B. Sarkar, D. Hou, X. Cao, E. Meers, J. Rinklebe, K.H. Kim, Y.S. Ok, Occurrence of contaminants in drinking water sources and the potential of biochar for water quality improvement: a review, *Crit. Rev. Env. Sci. Technol.*, 50 (2020) 549–611.
- [47] N.R. Draper, D.K.J. Lin, Response Surface Designs, S. Ghosh, C.R. Rao, Eds., Design and Analysis of Experiments. Handbook of Statistics, Vol. 13., North-Holland, 1996, pp. 343–375, doi: 10.1016/S0169-7161(96)13013-3.
- [48] A. Klimek-Kopyra, U. Sadowska, M. Kuboń, M. Gliniak, J. Sikora, Sunflower husk biochar as a key agrotechnical factor enhancing sustainable soybean production, *Agriculture*, 11 (2021) 305, doi: 10.3390/agriculture11040305.
- [49] K. Gondek, M. Mierzwa-Hersztek, M. Kopeć, J. Sikora, T. Głąb, K. Szczurowska, Influence of biochar application on reduced acidification of sandy soil, increased cation exchange capacity, and the content of available forms of K, Mg, and P, *Pol. J. Environ. Stud.*, 28 (2019) 103–111, doi:10.15244/pjoes/81688.
- [50] A. Kubaczyński, A. Walkiewicz, M. Brzezińska, B. Usowicz, How Does Biochar Affect Soil Respiration?, EGU General Assembly 2020, 4–8 May 2020, EGU2020-13343, doi: 10.5194/egusphere-egu2020-13343.
- [51] X. Yang, Q. Zheng, M. He, B. Chen, B. Hu, Bromine and iodine species in drinking water supply system along the Changjiang River in China: occurrence and transformation, *Water Res.*, 202 (2021) 117401, doi: 10.1016/j.watres.2021.117401.
- [52] F.M.D. Chequer, G.A.R. de Oliveira, E.R.A. Ferraz, J.C. Cardoso, M.V.B. Zanoni, D.P. de Oliveira, *Textile Dyes: Dyeing Process and Environmental Impact*, M. Günay, Ed., Eco-Friendly Textile Dyeing and Finishing, InTechOpen, 2013, pp. 151–176.
- [53] <https://pubchem.ncbi.nlm.nih.gov/> (Access date 30.11.2022)
- [54] Polish Standard PN-EN ISO 18134-2:2017-03, Solid Biofuels–Determination of Moisture Content–Oven Dry Method–Part 2: Total Moisture–Simplified Method, The Polish Committee for Standardization, Warsaw, Poland, 2017.
- [55] Polish Standard PN-ISO 1171:2002, Solid Mineral Fuels. Determination of Ash, The Polish Committee for Standardization, Warsaw, Poland, 2002.
- [56] A. Ramirez, R. Ocampo, S. Giraldo, E. Padilla, E. Flórez, N. Acelas, Removal of Cr(VI) from an aqueous solution using an activated carbon obtained from teakwood sawdust: kinetics, equilibrium, and density functional theory calculations, *J. Environ. Chem. Eng.*, 8 (2020) 103702, doi: 10.1016/j.jece.2020.103702.
- [57] Polish Standard PN-EN ISO 18123:2016-01, Solid Biofuels. Determination of The Content of Volatile Matter, The Polish Committee for Standardization, Warsaw, Poland, 2018.
- [58] Polish Standard PN 83/C-97555.04:1983, Activated Carbons, Methods of Tests, Determination of Adsorption Value of Iodine, The Polish Committee for Standardization, Warsaw, Poland, 2013.
- [59] S.S. Tripathy, S.B. Kanungo, Adsorption of  $\text{Co}^{2+}$ ,  $\text{Ni}^{2+}$ ,  $\text{Cu}^{2+}$  and  $\text{Zn}^{2+}$  from 0.5M NaCl and major ion sea water on a mixture of  $\delta\text{-MnO}_2$  and amorphous  $\text{FeOOH}$ , *J. Colloid Interface Sci.*, 284 (2005) 30–38.
- [60] Z.L. Zhu, H.M. Ma, R.H. Zhang, Y.X. Ge, J.F. Zhao, Removal of cadmium using  $\text{MnO}_2$  loaded D301 resin, *J. Environ. Sci.*, 19 (2007) 652–656.
- [61] A. Mannan, A.J. Khan, M. Khan, G. Abbas, S. Roohullah, M. Hussain, Spectrophotometric estimation of polyvinylpyrrolidone, iodate and iodine simultaneously in

- povidone-iodine complex in pure and pharmaceutical preparations, *RADS J. Pharm. Pharm. Sci.*, 7 (2019) 84–89.
- [62] Y.S. Ho, J.C.Y. Ng, G. McKay, Kinetics of pollutant sorption by biosorbents: review, *Sep. Purif. Rev.*, 29 (2000) 189–232.
- [63] P.S. Ghosal, A.K. Gupta, Determination of thermodynamic parameters from Langmuir isotherm constant-revisited, *J. Mol. Liq.*, 225 (2017) 137–146.
- [64] Y. Wang, Y. Hu, X. Zhao, S. Wang, G. Xing, Comparisons of biochar properties from wood material and crop residues at different temperatures and residence times, *Energy Fuels*, 27 (2013) 5890–5899.
- [65] K.B. Cantrell, P.G. Hunt, M. Uchimiya, J.M. Novak, K.S. Ro, Impact of pyrolysis temperature and manure source on physicochemical characteristics of biochar, *Bioresour. Technol.*, 107 (2012) 419–428.
- [66] X. Li, Q. Shen, D. Zhang, X. Mei, W. Ran, Y. Xu, G. Yu, Functional groups determine biochar properties (pH and EC) as studied by two-dimensional  $^{13}\text{C}$  NMR correlation spectroscopy, *PLoS One*, 8 (2013) e65949, doi: 10.1371/journal.pone.0065949.
- [67] A. Budai, L. Wang, M. Gronli, L.T. Strand, M.J. Antal Jr., S. Abiven, A. Dieguez-Alonso, A. Anca-Couce, D.P. Rasse, Surface properties and chemical composition of corn cob and miscanthus biochars: effects of production temperature and method, *J. Agric. Food Chem.*, 62 (2014) 3791–3799.
- [68] K. Intani, S. Latif, A.K.M. Rafayatul Kabir, J. Müller, Effect of self-purging pyrolysis on yield of biochar from maize cobs, husks and leaves, *Bioresour. Technol.*, 218 (2016) 541–551.
- [69] S.X. Zhao, N. Ta, X.D. Wang, Effect of temperature on the structural and physicochemical properties of biochar with apple tree branches as feedstock material, *Energies*, 10 (2017) 1293, doi: 10.3390/en10091293.
- [70] L.C. Malucelli, G.F. Silvestre, J. Carneiro, E.C. Vasconcelos, M. Guiotoku, C.M.B.F. Maia, M.A.S. Carvalho Filho, Biochar higher heating value estimative using thermogravimetric analysis, *J. Therm. Anal. Calorim.*, 139 (2019) 2215–2220.
- [71] L. Leng, Q. Xiong, L. Yang, H. Li, Y. Zhou, W. Zhang, S. Jiang, H. Li, H. Huang, An overview on engineering the surface area and porosity of biochar, *Sci. Total Environ.*, 763 (2021) 144204, doi: 10.1016/j.scitotenv.2020.144204.
- [72] H. Singh, B.K. Northup, Ch.W. Rice, P.V. Vara Prasad, Biochar applications influence soil physical and chemical properties, microbial diversity, and crop productivity: a meta-analysis, *Biochar*, 4 (2022), doi: 10.1007/s42773-022-00138-1.
- [73] M.B. Shaker, M.R. Fenjan, Characterization of biochar produced from sunflower seed husks (*Helianthus annuus*), *J. Adv. Mater. Eng.*, 7 (2022) 51–57.
- [74] W. Suliman, J.B. Harsh, N.I. Abu-Lail, A.M. Fortuna, I. Dallmeyer, M. Garcia-Perez, Influence of feedstock source and pyrolysis temperature on biochar bulk and surface properties, *Biomass Bioenergy*, 84 (2016) 37–48.
- [75] O. Duman, E. Ayranci, Adsorption characteristics of benzaldehyde, sulphanic acid, and p-phenolsulfonate from water, acid, or base solutions onto activated carbon cloth, *Sep. Sci. Technol.*, 41 (2006) 3673–3692.
- [76] E. Ayranci, O. Duman, Adsorption of aromatic organic acids onto high area activated carbon cloth in relation to wastewater purification, *J. Hazard. Mater.*, 136 (2006) 542–552.
- [77] S. Fan, Y. Wang, Z. Wang, J. Tang, J. Tang, X. Li, Removal of methylene blue from aqueous solution by sewage sludge-derived biochar: adsorption kinetics, equilibrium, thermodynamics and mechanism, *J. Environ. Chem. Eng.*, 5 (2017) 601–611.
- [78] M.A. Franciski, E.C. Peres, M. Godinho, D. Perondi, E.L. Foletto, G.C. Collazzo, G.L. Dotto, Development of  $\text{CO}_2$  activated biochar from solid wastes of a beer industry and its application for methylene blue adsorption, *Waste Manage.*, 78 (2018) 630–638.
- [79] V. Vadivelan, K.V. Kumar, Equilibrium, kinetics, mechanism, and process design for the sorption of methylene blue onto rice husk, *J. Colloid Interface Sci.*, 286 (2005) 90–100.
- [80] M.B. Ahmed, J.L. Zhou, H.H. Ngo, W. Guo, M.A.H. Johir, D. Belhaj, Competitive sorption affinity of sulfonamides and chloramphenicol antibiotics toward functionalized biochar for water and wastewater treatment, *Bioresour. Technol.*, 238 (2017) 306–312.
- [81] O. Duman, E. Ayranci, Adsorptive removal of cationic surfactants from aqueous solutions onto high-area activated carbon cloth monitored by *in-situ* UV spectroscopy, *J. Hazard. Mater.*, 174 (2010) 359–367.
- [82] T. Tian, S. Sun, Low-carbon transition pathways in the context of carbon-neutral: a quadrilateral evolutionary game analysis, *J. Environ. Manage.*, 322 (2022) 116105, doi: 10.1016/j.jenvman.2022.116105.
- [83] H. Li, V.L. Budarin, J.H. Clark, M. North, X. Wu, Rapid and efficient adsorption of methylene blue dye from aqueous solution by hierarchically porous, activated carbons: mechanism and porosity dependence, *J. Hazard. Mater.*, 436 (2022) 129174, doi: 10.1016/j.jhazmat.2022.129174.
- [84] G.Ch. Hill Jr., T.W. Root, *Introduction to Chemical Engineering Kinetics and Reactor Design*, John Wiley & Sons, Inc., New Jersey, 2014, pp. 153–156.
- [85] A. Subratti, J.L. Vidal, L.J. Lalgee, F.M. Kerton, N.K. Jalsa, Preparation and characterization of biochar derived from the fruit seed of *Cedrela odorata* L and evaluation of its adsorption capacity with methylene blue, *Sustain. Chem. Pharm.*, 21 (2021) 100421, doi: 10.1016/j.scp.2021.100421.
- [86] S. Liu, J. Li, S. Xu, M. Wang, Y. Zhang, X. Xue, A modified method for enhancing adsorption capability of banana pseudostem biochar towards methylene blue at low temperature, *Bioresour. Technol.*, 282 (2019) 48–55.
- [87] L. Lonappan, T. Rouissi, R.K. Das, S.K. Brar, A.A. Ramirez, M. Verma, R.Y. Surampalli, J.R. Valero, Adsorption of methylene blue on biochar microparticles derived from different waste materials, *Waste Manage.*, 49 (2016) 537–544.
- [88] L. Delgado-Moreno, S. Bazhari, G. Gasco, A. Méndez, M. El Azzouzi, E. Romero, New insights into the efficient removal of emerging contaminants by biochars and hydrochars derived from olive oil wastes, *Sci. Total Environ.*, 752 (2021) 141838, doi: 10.1016/j.scitotenv.2020.141838.
- [89] V. Choudhary, L. Philip, Sustainability assessment of acid-modified biochar as adsorbent for the removal of pharmaceuticals and personal care products from secondary treated wastewater, *J. Environ. Chem. Eng.*, 10 (2022) 107592, doi: 10.1016/j.jece.2022.107592.

### Supporting information

The optimization of adsorption conditions was based on central composite design (CCD) method, which is often used as a kind of response surface methodology (RSM). In the considered case the independent variables were:

- the initial concentration of adsorbate  $C_i$ : 10–250 mg/dm<sup>3</sup> for MB, 10–60 mg/dm<sup>3</sup> for PVP-I,
- adsorbent mass  $m_a$ : 0.1–0.6 g per 0.1 dm<sup>3</sup> of solution,
- the initial pH of the solution: 3–11.

Each independent variable  $X$  is expressed in normalized form. If  $X_{\min}$  and  $X_{\max}$  are the minimum and maximum value of  $X$ , then the normalized variable  $x$  corresponding to  $X$  equals:

$$x = 2\alpha \frac{X - \bar{X}}{\Delta X} \tag{S1}$$

where  $\bar{X} = \frac{X_{\max} + X_{\min}}{2}$  – the mean value,  $\Delta X = (X_{\max} - X_{\min})$  – the range of  $X$ , and  $\alpha$  is a coefficient, which for three variables equals  $2^{(3/4)} \approx 1.68$ . The inverse transformation is as follows:

$$X = \bar{X} + \frac{x}{2\alpha} \Delta X \tag{S2}$$

The CCD requires 5 levels of each variable.

$x$	$-\alpha$	$-1$	$0$	$1$	$\alpha$
$X$	$X_{\min}$	$\bar{X} - \frac{\Delta X}{2\alpha}$	$\bar{X}$	$\bar{X} + \frac{\Delta X}{2\alpha}$	$X_{\max}$

If full design was used, five levels for three variables would result in  $5^3 = 125$  sampling points, but the CCD results in 15 different sampling points. However, 20 samples are used, because the central point (0, 0, 0) is used 6 times to reduce the error for mean values. In the considered case the values of independent variables, both physical and normalized, are in columns 1–7 of Table 5 in the main body of the manuscript.

In the next step for each sampling point adsorption was performed. Then the equilibrium concentration of adsorbate ( $C_e$ ) was measured, and the removal efficiency was calculated as follows:

$$E = \left( \frac{C_i - C_e}{C_i} \right) \times 100\% \tag{S3}$$

This was the dependent variable, which was then subject to maximization. For this purpose, the following approximation was used:

$$\begin{aligned} \tilde{E} = & a_0 + a_1x_1 + a_2x_2 + a_3x_3 + a_4x_1x_2 + a_5x_1x_3 \\ & + a_6x_2x_3 + a_7x_1^2 + a_8x_2^2 + a_9x_3^2 \end{aligned} \tag{S4}$$

where  $a_0$  to  $a_9$  are unknown coefficients, whereas  $x_1, x_2$  and  $x_3$  are the normalized independent variables. Hence, the problem is to:

- find  $a_0$  to  $a_9$  by minimizing the residual sum of squares:

$$RSS = \sum_{i=1}^n (\tilde{E}(x_1, x_2, x_3) - E_i)^2 = \min \Rightarrow a_0, a_1, \dots, a_9 \tag{S5}$$

- find maximum of  $\tilde{E}$ .

In the first step, the linear regression method is used to find coefficients  $a_0$  to  $a_9$ . To assess the goodness of fit the so-called adjusted  $R^2$  is used, which is defined as follows:

$$R^2_{\text{adj}} = 1 - \left[ \frac{(1 - R^2)(n - 1)}{n - k - 1} \right] \tag{S6}$$

where  $R^2$  is the “usual”  $R^2$ ,  $n$  is number of sampling points,  $k$  is the number of parameters in the model (excluding the constant term). This penalizes the number of terms in the regression model for  $\tilde{E}$ , and allows for taking into account significant basis functions, only.

In the considered case we performed calculations for all subsets of the basis functions  $\{1, x_1, x_2, x_3, x_1x_2, x_3x_1, x_1^2, x_2^2, x_3^2\}$  and selected that of maximal  $R^2_{\text{adj}}$ . The results are shown in Table 6, where coefficients for methylene blue (MB) and povidone-iodine (PVP-I) are shown for the highest  $R^2_{\text{adj}}$  (not used terms are omitted). The obtained approximations of efficiency for MB and PVP-I adsorption are as follows:

$$\tilde{E}_{\text{MB}} = 95.9 - 2.45x_1 + 1.50x_2 + 0.61x_1^2 - 2.68x_2^2 \tag{S7}$$

$$\tilde{E}_{\text{PVP-I}} = 13.8 - 8.26x_1 + 6.26x_2 + 13.6x_1^2 \tag{S8}$$

These are the best possible fits with respect to  $R^2_{\text{adj}}$ . They are plotted in Fig. 4a and b, respectively

Step 2) Having found  $\tilde{E}$ , it is possible to localize the maximum.

Function  $\tilde{E}_{\text{MB}}$  depends on  $x_1$  and  $x_2$ , whereas no term with  $x_3$  is present. This means that pH weakly affected the removal efficiency. This allows us plotting the function in  $(x_1, x_2)$  coordinates – Fig. 4a. The maximum can be easily located at point  $(-\alpha, 0.28, 0)$ , which corresponds to the lowest concentration and adsorbent mass around 0.4 g per 0.1 dm<sup>3</sup>. What is interesting, as the concentration changes, the removal efficiency remains best for mass 0.4 g. Therefore, in further experiments the adsorbent mass for MB adsorption was established at this level.

Function  $\tilde{E}_{\text{PVP-I}}$  is more ambiguous. Nevertheless, the coefficient related with  $x_2$  (adsorbent mass) is positive, which indicates that the higher mass of adsorbent the higher removal efficiency. Therefore, the adsorbent mass was established to the maximum tested one (0.6 g per 0.1 dm<sup>3</sup> of solution).